Arabian Journal of Chemistry (2022) **15**, 104105

King Saud University

Arabian Journal of Chemistry

www.ksu.edu.sa
www.sciencedirect.com

ORIGINAL ARTICLE

Construction of hydroxyethyl cellulose/silica/graphitic carbon nitride solid foam for adsorption and photocatalytic degradation of dyes

Zhong-Zheng Gao [a], Na Qi [b], Wen-Jie Chen [a], Hui Zhao [a,*]

[a] *College of Chemical and Biological Engineering, Shandong University of Science and Technology, 579 Qianwangang Road, Huangdao District, 266590, Qingdao, Shandong Province, PR China*
[b] *School of Chemistry and Chemical Engineering, Shandong University, 27 South Road of ShanDa, 250100, Jinan, Shandong Province, PR China*

Received 19 May 2022; accepted 4 July 2022
Available online 8 July 2022

KEYWORDS

Hierarchical solid foam;
Adsorption;
Photocatalytic degradation;
Dye removal

Abstract In the present study, novel hydroxyethyl cellulose/silica/graphitic carbon nitride (HEC/SiO_2/C_3N_4) solid foams with hierarchical porous structure have been successfully fabricated with gas bubbles template combination with freeze-drying method. Compared with HEC/SiO_2/C_3N_4-50 without gas foaming, the HEC/SiO_2/C_3N_4-80 with air bubbles template had larger pore volume and higher porosity and specific surface area, which not only exhibited faster adsorption rate, but also presented higher saturated adsorption capacity towards methylene blue (MB) and methyl violet (MV). From the experimental results, it was found that HEC/SiO_2/C_3N_4-80 had high adsorption capacities of 132.45 mg/g and 206.62 mg/g for MB and MV, respectively, and the adsorption process fitted the Langmuir adsorption isotherm and pseudo-second-order rate equation. Additionally, benefiting from its higher adsorption capacity and light-harvesting capability, HEC/SiO_2/C_3N_4-80 exhibited relatively higher photocatalytic degradation efficiencies against MB and MV under visible light irradiation than HEC/SiO_2/C_3N_4-50. More importantly, compared with the bare g-C_3N_4 powder, the HEC/SiO_2/C_3N_4 solid foams could be more easily separated from the treated water, which facilitated their recycle and reuse. Therefore, the good adsorption capacity, high photocatalytic degradation activity and recyclability of the HEC/SiO_2/C_3N_4 solid foam made it a promising candidate for the removal of organic dyes from wastewater.

* Corresponding author.at: College of Chemical and Biological Engineering, Shandong University of Science and Technology, 579 Qianwangang Road, Huangdao District, 266590, Qingdao, Shandong Province, PR China
E-mail address: zhaohui7592@sdust.edu.cn (H. Zhao).

Peer review under responsibility of King Saud University.

Production and hosting by Elsevier

https://doi.org/10.1016/j.arabjc.2022.104105
1878-5352

1. Introduction

Organic dyes have been widely used in the industrial coloring processes, such as paper, cosmetics, textile, and printing, etc. However, a large number of dyes are directly released into the surrounding water bodies without fully utilized. Owing to their toxicity and non-biodegradability, organic dyes create tremendous threats to the human health and environment. Therefore, the efficient removal of dyes from wastewater by ecofriendly techniques is imperative and necessary. Different methods have been developed such as photocatalytic degradation, chemical precipitation and physical adsorption and so on (Das et al., 2017, Jiao et al., 2020, Liu et al., 2021). But the sole employment of each method presented some limitations, e.g., limited photocatalytic efficiency, low adsorption. Therefore, it is necessary to explore materials synergizing high photocatalytic activities and good adsorption properties for dye removal (Yang et al., 2017).

Graphitic carbon nitride (g-C_3N_4), an attractive semiconductor material, has aroused considerable attention in photocatalytic fields, owing to its good stability, low cost, nontoxicity and outstanding photocatalytic property (Jin et al., 2019). However, the poor adsorption ability and difficulty in separation performance retard its practical applications (Hao et al., 2018). Porous materials such as hydrogel, aerogel, solid foam, are effective catalyst supports as they can not only improve the recycling performance of the catalyst, but also synergize their strong adsorption ability and high photocatalytic efficiency of photocatalyst (Qi et al., 2019, Tan et al., 2019). Therefore, introducing g-C_3N_4 into the porous materials is a wise choice to optimize its performance. Compared with the common porous materials, hierarchically porous materials with tunable porous structures, controllable macroscopic morphologies and adjustable multiple functions exhibit obvious superiority (Bai et al., 2015, Yousefi et al., 2018, Dai et al., 2020). On the one hand, introduction of meso and macroporosity in materials can improve surface area and mass transport, and promote the reactant molecules migrate to photocatalytic active sites(Yang et al., 2017). On the other hand, the macropores can enhance light scattering and light absorption, thereby improving the photocatalytic activity (Parlett et al., 2013).

Templating method is the most commonly employed strategy for designing hierarchically porous materials, which includes the templates of emulsion, colloidal crystal, nanoparticles and so on (Barbetta et al., 2009, Lau et al., 2014). But these conventional templates either involve consuming extensive toxic organic solvent or require complex post-treatment processes, limiting their applications. As a novel template, gas bubbles exhibit great promise in constructing porous materials, benefiting from their unique properties of environment-friendly, low-cost and easy-preparation. Moreover, the regulation of materials' microscopic structures and functionalities could be realized through controlling over the bubbles' size and shape (Lesov et al., 2014).

In the present study, hydroxyethyl cellulose/silica/graphitic carbon nitride (HEC/SiO_2/C_3N_4) solid foams with hierarchical structures were constructed for efficient removal of organic dyes in wastewater. Hydroxyethyl cellulose, a typical cellulose derivative with superior physical properties of excellent water solubility, chemical stability, good biocompatibility and biodegradability, has been explored to removal heavy metals from polluted water (Jilal et al., 2018). Ludox®,a silica-based nanoparticle, presents advantages of environmental friendly and low cost, which is reported to interact with DNA for constructing stable hydrogel (25 wt% Ludox® with 5 wt% DNA) (Bagley and Jones 2021). Here, Ludox® TM-50 with an average size of 22 nm was selected as the crosslinking agent to design HEC/SiO_2 solid foam matrix for the loading of g-C_3N_4. To design the hierarchically HEC/SiO_2/C_3N_4 solid foam, the strategies of gas bubbles template combination with freeze-drying method were introduced. An anionic surfactant, sodium dodecyl sulfate (SDS), was chosen as the foaming agent and bubbles stabilizer. After mechanically foaming and cooling down of the hot HEC/SiO_2/C_3N_4 sol solution, the generated bubbles were successfully solidified in the formed HEC/SiO_2/C_3N_4 hydrogel. After freeze-drying, the hierarchically HEC/SiO_2/C_3N_4 solid foam was obtained. Then the formation mechanism, adsorption behavior and photocatalytic activity of HEC/SiO_2/C_3N_4 solid foam were systematically investigated.

2. Experimental section

2.1. Materials

Hydroxyethyl cellulose (HEC, 98%, with Mw of ~ 1300 kDa) and benzoquinone (BQ, 99.0%) were purchased from Macklin. Sodium dodecyl sulfate (SDS, 98.5%), methylene blue (MB, 98.0%), methyl violet (MV, 98.0%) and disodium EDTA (EDTA-2Na, 99.0%) were purchased from Sinopharm Chemical Reagent Co.,Ltd. Ludox®TM-50 (colloidal silica, 50 wt %) was obtained from Aladdin Reagent Co., Ltd. Graphite carbon nitride (g-C_3N_4) was purchased from Bonte Chemical Co., Ltd. Tert-Butanol (t-BuOH) was purchased from Tianjin Fuyu Co., Ltd.

2.2. Preparation of HEC/SiO_2 hydrogel

HEC/SiO_2 hydrogel was prepared by a physical cross-linking method according to the following process (Gong et al., 2019). Firstly, 25 g HEC solution (2 wt%), 10 g Ludox®TM-50 and 15 g ultra-pure water were mixed together and stirred vigorously at 90℃for 15 min to form a homogeneous sol solution. Then the sol solution was transferred to a glass mould which was cooled down at 20℃. After 30 min, the HEC/SiO_2 hydrogel was successfully formed. The schematic diagram of preparation of HEC/SiO_2 hydrogel was shown in Scheme 1.

2.3. Preparation of HEC/SiO_2/C_3N_4 solid foam

HEC/SiO_2/C_3N_4 foam was synthesized as follows. As shown in Scheme 2, firstly, 0.2 g g-C_3N_4 powder and SDS were dispersed into 15 g ultra-pure water with 2 h of ultrasonic dispersion to form homogeneous SDS/C_3N_4 solution (c_{SDS} = 20 mM). Then, the SDS/C_3N_4 solution was mixed with 25 g of HEC solution (2 wt%) and 10 g Ludox®TM-50 which were placed into water bath (90℃) and stirred magnetically for 15 min, obtaining the homogeneous sol solution. Subsequently, the sol solution was magnetically foamed with a stainless steel milk beater (no: 50172661550) for 10 min to produce enough air bubbles. The volume of the produced liquid foam emulsion was 80 mL. After cooling down for 30 min at 20℃, the aqueous foam was cross-linked which was then freeze-dried in a vacuum freeze dryer (FD-1A-50+, Beijing Boyikang Co., Ltd.) for 48 h (1 Pa, −50℃), generating HEC/SiO_2/C_3N_4-80 solid foam. Additionally, for comparison, the sample prepared without magnetically foaming was marked as HEC/SiO_2/C_3N_4-50.

2.4. Determination of the porosity of HEC/SiO_2/C_3N_4 solid foam

The porosity of the obtained solid foam was calculated by the following equation (Huang et al., 2018):

$$\text{porosity}\ (\%) = \left(1 - d_p/d_b\right) \times 100$$

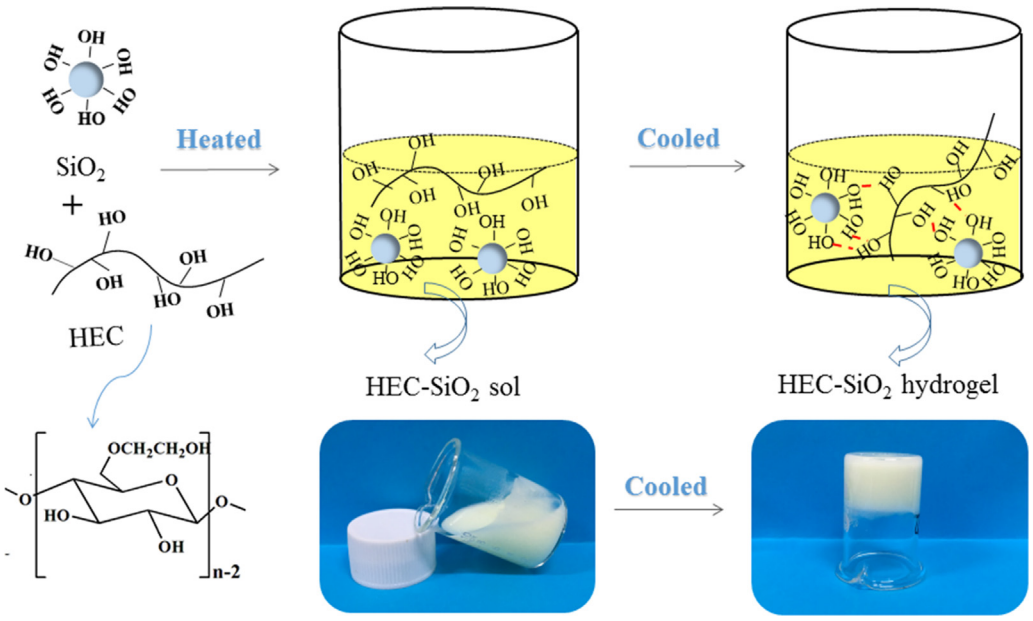

Scheme 1 Schematic diagram of preparation of HEC/SiO_2 hydrogel.

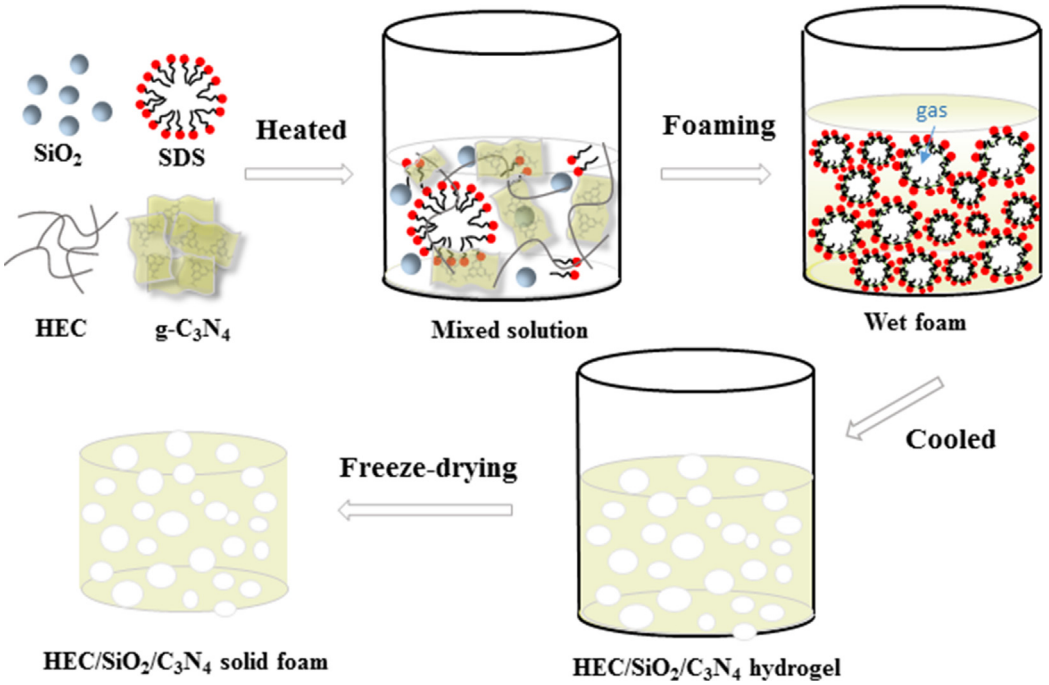

Scheme 2 Schematic diagram of preparation of HEC/SiO_2/C_3N_4 solid foam.

where d_p was the density of the solid foam and d_b was the density of the bulk SiO_2 (2.2 g/cm^3). The density of the solid foam (d_p) was determined from the ratio of mass to volume.

2.5. Dye adsorption and photocatalytic experiments

Adsorption kinetics study. The dye adsorption experiment was carried out at room temperature and MB and MV were taken as the model pollutants in the experiment. 0.05 g sample was placed in 30 mL dye solution (10 mg/L), and 0.5 mL dye solution was withdrawn at certain time and its concentration was determined by UV–vis spectroscopy (Shimadzu UV-1800). The adsorption capacity at time t (q_t) was calculated according to the following equation:

$$q_t = \frac{(c_0 - c_t)V}{m}$$

where c_0 (mg/L) was the initial concentration of the dye solution, c_t (mg/L) was the concentration of dye solution at time t,

V (mL) was the volume of dye solution and m (g) was the weight of the solid foam.

Adsorption isotherm study. 0.05 g sample was placed into 20 mL of dye solutions with different concentrations (20 ~ 1200 mg/L). After adsorption for 6 h, the sample was taken out from the solutions. The saturated adsorption capacity (q_e) was calculated according to the following equation:

$$q_e = \frac{(c_0 - c_e)V}{m}$$

where c_e (mg/L) was the equilibrium concentration of dye solution.

Photocatalytic degradation of dyes. The dye solution with the initial concentration of 30 mg/L was used for the photocatalytic degradation experiment. 0.05 g sample was placed into 20 mL of dye solution in dark for 30 min to allow the adsorption of MB or MV into HEC/SiO_2/C_3N_4. After adsorption, the dye solution was placed in a photoreactor equipped with a 300 W Xenon lamp (CEL-HXF300, Beijing Zhongjiaojinyuan Co., Ltd.) (780⟩ λ > 420 nm) with a cutoff filter of 420 nm to attenuate UV irradiation. The real-time concentration of the dye solution was determined by UV–vis spectroscopy.

2.6. Characterization

FT-IR spectra of HEC/SiO_2 was analyzed by a Nicolet FT-IR iS50 spectrometer with Attenuated Total Reflectance (ATR) accessory. The morphology of the sample was characterized by scanning electron microscopy (SEM, JEM-6700F, BRUKER). Nitrogen adsorption–desorption isotherms were given by the surface aera analyzer (ASAP 2460, Micromeritics Instrument Ltd.). The specific surface aera was calculated according to the Brunauer-Emmett-Teller (BET) equation and the pore size distribution was obtained by applying the Non-Localized Density Functional Theory (NL-DFT) method to the adsorption isotherms (Bao et al., 2022).

3. Results and discussion

3.1. Preparation and characterization of HEC/SiO_2 hydrogel

As shown in Scheme 1, the mixed solution of HEC and Ludox®TM-50 presented liquid-like property with obvious fluidity under 90℃. During the cooling process at 20℃, the fluidity of the solution weakened gradually and the HEC-SiO_2 sol turned into hydrogel eventually. The gelation time determined by an inversion method was 19 min, which was not only long enough to produce enough bubbles, but also short enough to ensure the stabilization of the generated air bubbles before the solidification (Andrieux et al., 2018, Zhao and Li 2020).

The formation mechanism of HEC/SiO_2 hydrogel was determined through FT-IR spectra. As shown in Figure S1, HEC presented obvious peaks at 3379 cm^{-1}, 2878 cm^{-1} and 1050 cm^{-1}, which were attributed to the stretching vibrations of O-H, C-H and C-O groups in pyranose ring, respectively (Jilal et al., 2018). For SiO_2 nanoparticles, the bands at 3652 cm^{-1} and 797 cm^{-1} represented symmetrical stretching vibration peaks of O-H and Si-O-Si groups, respectively (Mukerabigwi et al., 2016). In the spectrum of HEC/SiO_2, the characteristic absorption peaks of SiO_2 and HEC were both found and no newly formed chemical bonds were observed, indicating that the formation of HEC/SiO_2 hydrogel was based on physical interactions. According to our previous Density Functional Theory (DFT) calculations, which determined the hydrogen bonding interaction between the monomer of HEC and SiO_2 (Zhao et al., 2019), we speculated that the hydrogen bonding interactions between HEC and SiO_2 might contribute to the formation of HEC/SiO_2 hydrogel. Based on the obtained HEC/SiO_2 hydrogel, HEC/SiO_2/C_3N_4 solid foam with hierarchical structure was carefully designed which was discussed in detail in Section 3.2.

3.2. Preparation and characterization of HEC/SiO_2/C_3N_4 solid foam

Successful preparation of desired porous materials through gas bubbles template required generation of stable bubbles and matching the time scale between foaming process, stability of bubbles and the solidification of generated bubbles. According to the reference, SDS could efficiently stabilize air bubbles (Zhang et al., 2018), therefore, it was selected as a foaming agent and bubble stabilizer. As shown in Fig. 1a, not only abundant air bubbles were produced in HEC/SiO_2/C_3N_4 sol solution, but also the bubbles were stable enough during the gelation process. As the gelation time was only 19 min, the solidification of air bubbles into HEC/SiO_2/C_3N_4 hydrogel network before the bubbles' rupture was realized.

The porous HEC/SiO_2/C_3N_4 hydrogel was converted to HEC/SiO_2/C_3N_4 solid foam when it was freeze-dried for 48 h. As shown in Fig. 1c, the structure of the air bubbles was well preserved in HEC/SiO_2/C_3N_4-80 solid foam. The diameter of the pores in HEC/SiO_2/C_3N_4-80 ranged from about 200 μm to a few millimeters, which were a little larger than that of the air bubbles. This might be attributed to the slight coalescence and rupture of the air bubbles during the gelation process (Tan et al., 2018, Zhang et al., 2019). Furthermore, significant pore throats can be interestingly found between the adjacent pores, leading to an open-cell structure in HEC/SiO_2/C_3N_4-80, which will promote the diffusion and transport of dye molecules. For comparison, HEC/SiO_2/C_3N_4-50 solid foam was prepared under magnetic stirring, instead of mechanically foaming. As shown in Fig. 1b, only a few bubbles were produced in sol solution and the generated HEC/SiO_2/C_3N_4-50 foam presented irregular pore structures with a diameter of around 20–100 μm (Fig. 1d). This suggested that the gas foaming was helpful to the generation of supermacroporous structures.

The microstructure features of the HEC/SiO_2/C_3N_4 solid foams were further characterized by their nitrogen adsorption-desorption isotherms (Fig. 2a). Clearly, the solid foams presented type IV isotherms with H2 hysteresis loop, indicating the co-existence of mesopores and macropores (Nguyen and Juang 2019). Pore-size distribution curves of the solid foams in Fig. 2b also confirmed the existence of nano-scale pores. Therefore, it could be verified that hierarchical porous structures were produced in HEC/SiO_2/C_3N_4 solid foams, especially for HEC/SiO_2/C_3N_4-80, which even presented additional supermacroporous structures.

The specific surface areas of HEC/SiO_2/C_3N_4-50 and HEC/SiO_2/C_3N_4-80 were 38 m^2/g and 47 m^2/g, respectively (Fig. 2c), while the pore volumes were 0.33 cm^3/g and 0.39 cm^3/g, respectively. And their porosities were calculated to be 92% and

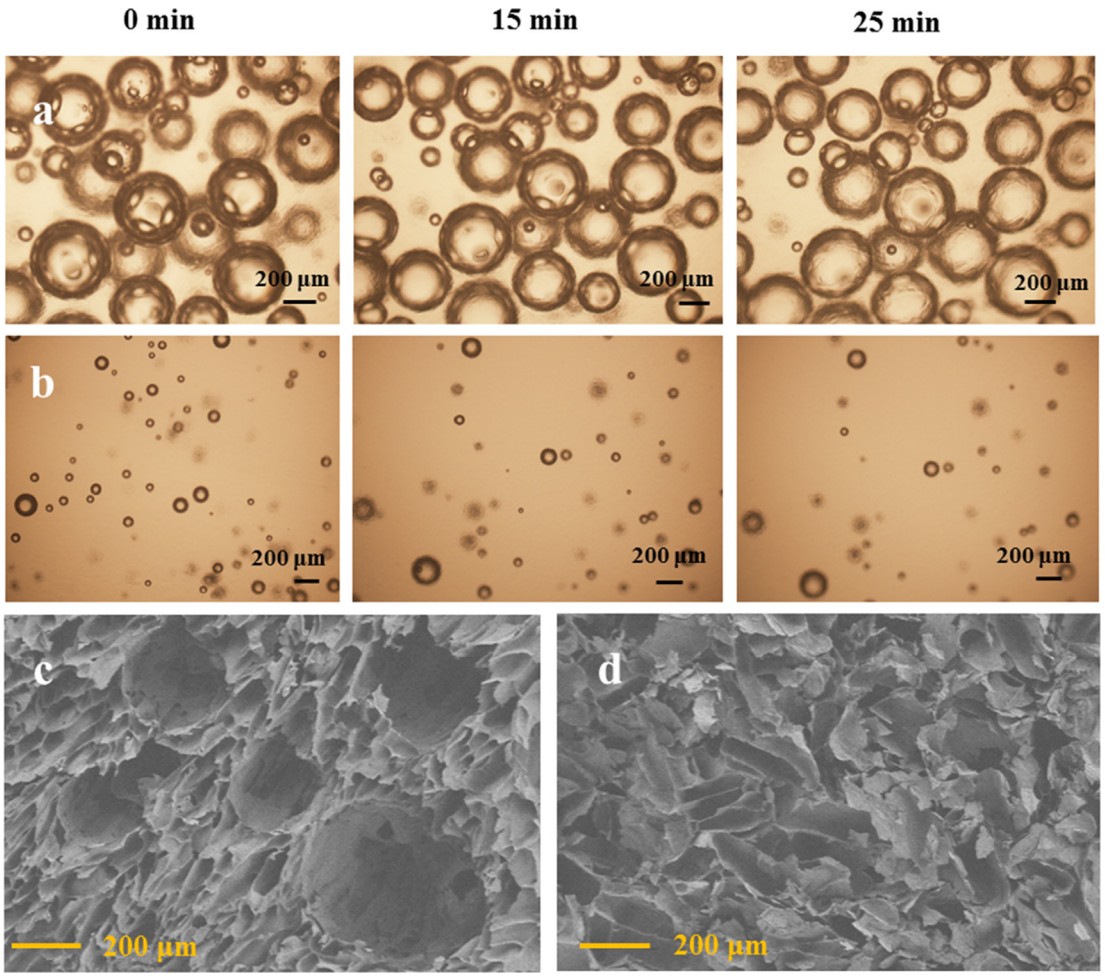

Fig. 1 Variations of the bubbles in HEC/SiO_2/C_3N_4 with time: (a) HEC/SiO_2/C_3N_4-80, (b) HEC/SiO_2/C_3N_4-50; SEM images of the different solid foams: (c) HEC/SiO_2/C_3N_4-80, (d) HEC/SiO_2/C_3N_4-50.

96%, respectively (Fig. 2d). Therefore, it can be concluded that the gas bubbles template could promote the increment of specific surface area, pore volume and porosity of the solid foam. Predictably, the hierarchical structures with open-cell pores, higher porosity, higher specific surface area and larger pore volume of HEC/SiO_2/C_3N_4-80 made it more suitable for wastewater treatment.

3.3. Adsorption of organic dye

The adsorption behavior of MB by HEC/SiO_2/C_3N_4 was investigated carefully. Fig. 3a gave the effect of contact time on the adsorption of MB. The adsorption process of MB onto HEC/SiO_2/C_3N_4 could be divided into three steps: initially, the adsorption rate of MB was very fast and the adsorption onto HEC/SiO_2/C_3N_4-80 was much faster than that onto HEC/SiO_2/C_3N_4-50; then, the adsorption of MB got to be slower, which was attributed to the gradual occupation of adsorption sites on HEC/SiO_2/C_3N_4, resulting in the slower diffusion of MB molecules to the solid foam; lastly, the adsorption of MB reached to equilibrium and the adsorption capacity hardly changed with time.

Pseudo-first-order and pseudo-second-order kinetic models as well as intra-particle diffusion model were employed to investigate the adsorption kinetic process of MB (S1.1 in Supporting Information) (Azizian 2004, Rudzinski and Plazinski 2006). The fitted parameters (Fig. 3b, Table S1) revealed that pseudo-second-order model described the adsorption behavior of MB well. According to this model, the calculated values of the initial adsorption rate ($h = k_2 q_e^2$) for MB adsorption on HEC/SiO_2/C_3N_4-50 and HEC/SiO_2/C_3N_4-80 were 0.1968 mg g^{-1}•min^{-1} and 1.8570 mg•g^{-1}•min^{-1}, respectively, indicating the higher initial adsorption rate of MB onto HEC/SiO_2/C_3N_4-80 (Chatterjee et al., 2009). The higher adsorption rate might be attributed to the larger specific surface area, higher porosity and larger pore volume of HEC/SiO_2/C_3N_4-80, which could promote the diffusion, transfer and adsorption of MB molecules (Ren et al., 2019). Clearly, the fitted results of intra-particle diffusion model (Figure S2) also confirmed the faster diffusion and adsorption of MB onto HEC/SiO_2/C_3N_4-80.

Compared with HEC/SiO_2/C_3N_4-50, HEC/SiO_2/C_3N_4-80 not only exhibited faster adsorption rate, but also presented higher saturated adsorption capacity towards MB. The adsorption isotherms demonstrated this point (Fig. 3c). The adsorption data was analyzed by Langmuir and Freundlich models(Fig. 3d, Table S2), which revealed that the adsorption of MB matched Langmuir model (Kinniburgh 1986, Ho et al.,

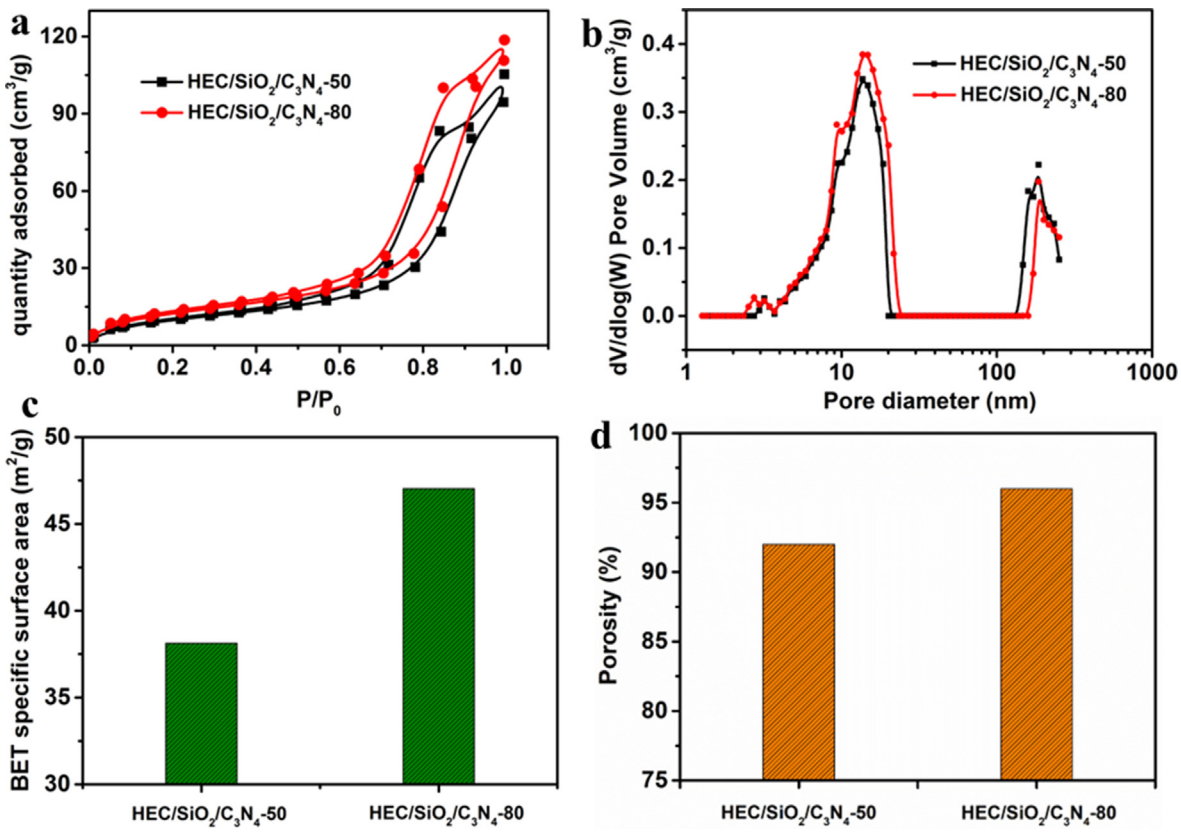

Fig. 2 (a) N_2 adsorption-desorption isotherms (b) pore size distribution calculated using DFT method (c) BET specific surface area (d) porosity of HEC/SiO_2/C_3N_4-50 and HEC/SiO_2/C_3N_4-80.

2002). On the basis of this model, the maximum adsorption capacities of MB onto HEC/SiO_2/C_3N_4-50 and HEC/SiO_2/C_3N_4-80 were 93.20 mg/g and 132.45 mg/g, respectively. The higher adsorption capacity of HEC/SiO_2/C_3N_4-80 might be benefited from its higher specific surface area which could provide more binding sites such as hydroxyl and triazine groups for the dye adsorption (Xu et al., 2022). Besides MB, the adsorption behavior of MV was also carefully investigated. From Figure S3 and Figure S4, it can be clearly seen that not only was the adsorption rate of MV by HEC/SiO_2/C_3N_4-80 faster, HEC/SiO_2/C_3N_4-80 had higher adsorption amount towards MV. Compared with the hydrogel reported in the previous literature (Table 1), it was clearly indicated that the obtained HEC/SiO_2/C_3N_4 solid foam exhibited relatively good adsorption performance. More importantly, compared with the bare g-C_3N_4, the HEC/SiO_2/C_3N_4 solid foams not only presented better adsorption performance (Figure S5), but also can be easily separated and collected from the treated water, which will be a promising and competitive candidate for the removal of organic dyes from wastewater.

3.4. Photocatalytic degradation of dyes

To investigate the photocatalytic degradation performance of HEC/SiO_2/C_3N_4, photocatalytic degradation of MB was carried out under visible light. After reaction for 60 min, the removal efficiency of MB (10 mg/L, 20 mL) was 94.6%, while it was only 68% in dark (Fig. 4a), demonstrating the excellent photocatalytic activity of HEC/SiO_2/C_3N_4. Then, the photocatalytic performance of the different solid foams was examined. HEC/SiO_2/C_3N_4 was firstly put into MB solution (30 mg/L, 20 mL) in dark for 30 min to allow the effective adsorption, and then was exposed to visible light. As shown in Fig. 4b, the degradation efficiencies of MB by HEC/SiO_2/C_3N_4-50 and HEC/SiO_2/C_3N_4-80 were 80.3% and 82.3% respectively. And the calculated corresponding rate constants (K_{app}) were 0.017 min^{-1} and 0.018 min^{-1}, indicating the relative higher photocatalytic activity of HEC/SiO_2/C_3N_4-80. Similar results were also obtained for the photocatalytic degradation of MV. As illustrated in Figure S6, the removal efficiencies of MV by HEC/SiO_2/C_3N_4-50 and HEC/SiO_2/C_3N_4-80 were 84.0% and 87.0% respectively. This might be due to that HEC/SiO_2/C_3N_4-80 not only presented higher adsorption capacity, but also showed larger specific surface area and higher porosity, which enhanced the light-harvesting capability (Figure S7) (Wang et al., 2018, Qian et al., 2019), thereby promoting its photocatalytic activity.

The stability and reusability of the catalyst was important for its practical application. Therefore, cycling tests were carried out to investigate the stability of HEC/SiO_2/C_3N_4 solid foam. The used solid foam was gathered from the reaction dye solution and then was washed thoroughly by ultrapure water to reuse. As shown in Figure S8, the removal efficiency of MB presented slightly decrease after four continuous cycles, confirming the relatively good stability and reusability of the HEC/SiO_2/C_3N_4 solid foam.

Different free radical scavengers were added into the reaction system to analyze the catalytic mechanism. Clearly, the

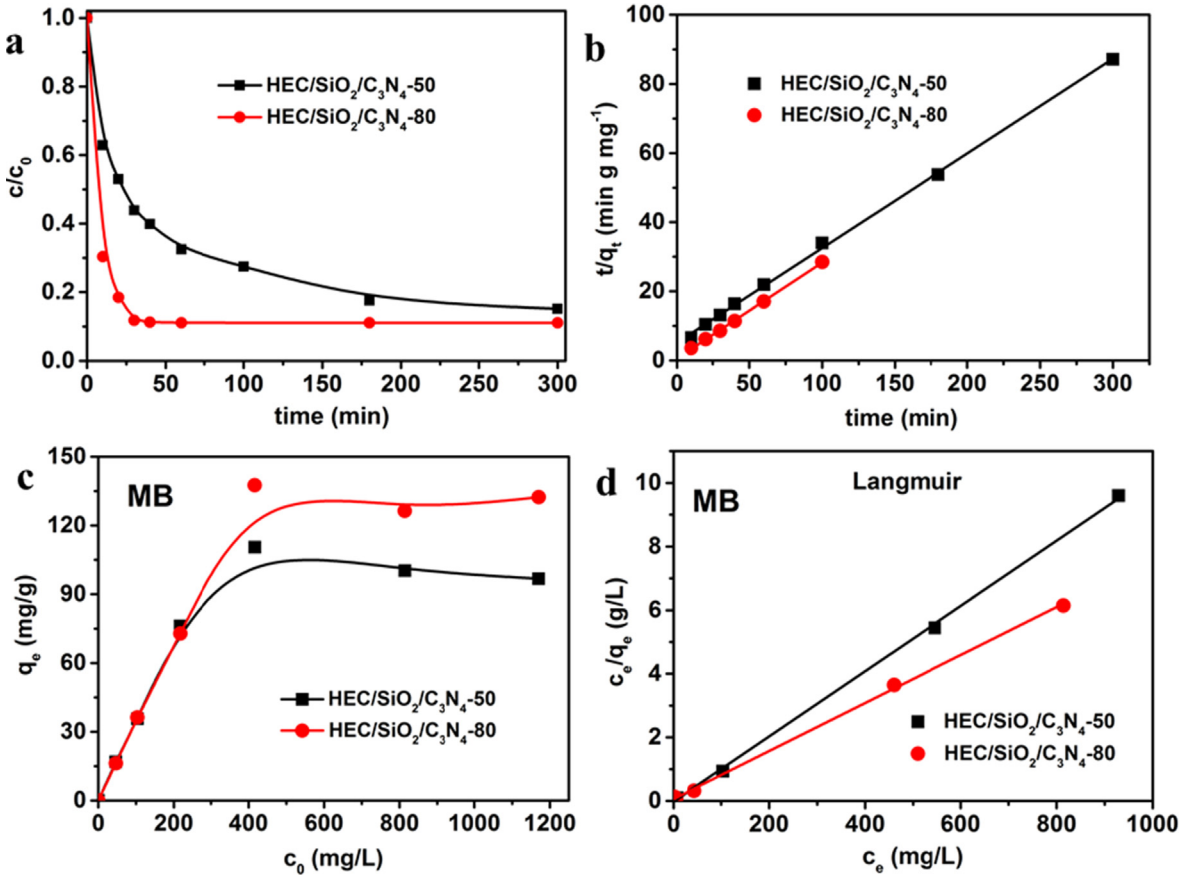

Fig. 3 (a) Effect of contact time on the adsorption of MB; (b)Plots of the pseudo-second-order kinetics model for the adsorption of MB; (c) Adsorption isotherms of MB; (d) Plots of Langmuir adsorption isotherm model for the adsorption of MB.

removal efficiency of MB presented little change with addition of t-BuOH, while it was slightly decreased when EDTA-2Na was added. However, the degradation of MB was inhibited significantly by benzoquinone (Figure S9). Therefore, it can be demonstrated that hydroxyl radicals (·OH) and holes (h^+) were not the main active species in the photocatalytic reaction, while $\cdot O_2^-$ played the major role in the photodegradation process of MB (Zhu et al., 2022). In HEC/SiO_2/C_3N_4, g-C_3N_4 was the main photocatalyst. Under visible light irradiation, g-C_3N_4 could adsorb photo energy, inducing excitation of electrons from valence band (VB) to conduction band (CB). The redox potential of OH^-/·OH [$E^0(OH^-/\cdot OH)$ = 2.29 eV, $E^0(H_2O/\cdot OH)$ = 2.38 eV] was more positive than that of the valence band of g-C_3N_4 (1.35 eV), therefore, the holes on the valence

Table 1 Adsorption capacities of different adsorbent for MB and MV in the literature.

Dye	Adsorbent	Adsorption capacity (mg/g)	Ref.
MB	Amphiphilic tris-urea hydrogel	2.58	(Takeshita et al., 2017)
	PAA-Ag/AgNPs hydrogel	7.56	(Hou et al., 2016)
	Guar gum-g-(AA-co-AM-co-APA)	27.06	(Singha et al., 2017)
	Polyaniline hydrogel	37.20	(Yan et al., 2015)
	Magadiite-chitosan hydrogel	45.25	(Mokhtar et al., 2020)
	Poly(AA-co-VPA) hydrogel	66.89	(Nakhjiri et al., 2018)
	This work (HEC/SiO_2/C_3N_4-80)	132.45	
MV	SA-g-PSMA hydrogel	109.9	(Eskhan et al., 2018)
	P(NIPAM-co-AA)/ATP hydrogel	168.35	(Liu et al., 2022)
	PAA-HEMA-SA hydrogel	172.0	(Mandal and Ray 2013)
	Salecan hydrogel	178.0	(Qi et al., 2019)
	GE-g-MMA/Gph hydrogel	250.0	(Chaudhary et al., 2021)
	Peach gum hydrogel	277.0	(Zhou et al., 2014)
	This work (HEC/SiO_2/C_3N_4-80)	206.62	

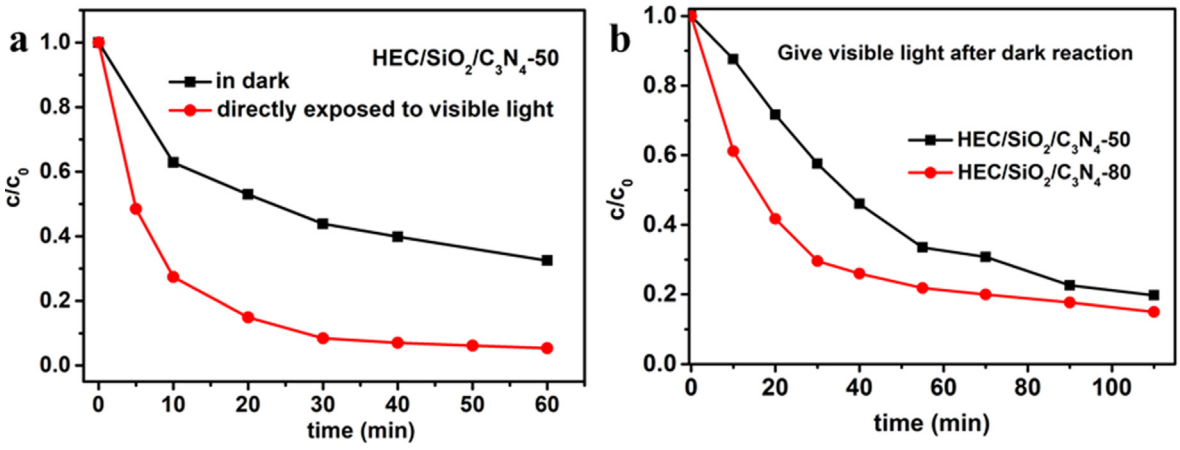

Fig. 4 (a) Removal efficiencies of MB by HEC/SiO_2/C_3N_4-50 in dark and under visible light irradiation directly; (b) Removal efficiencies of MB by different HEC/SiO_2/C_3N_4 solid foams.

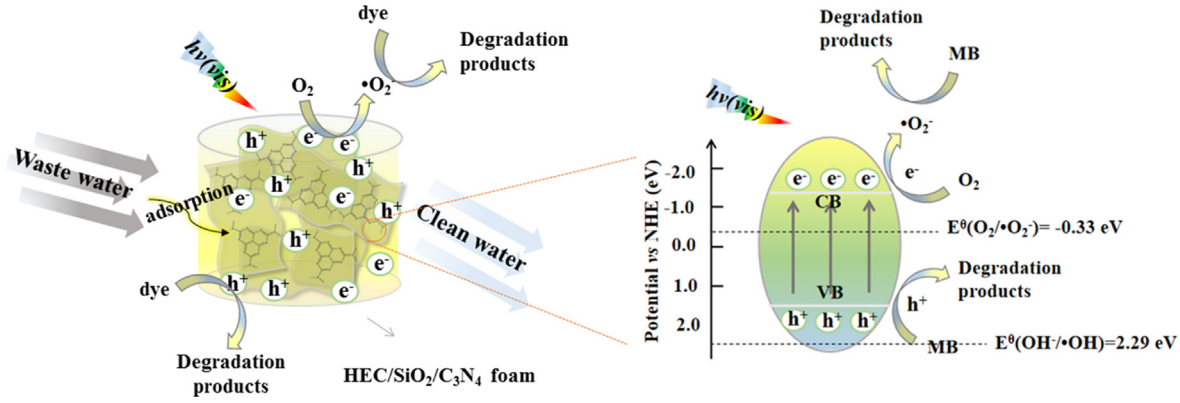

Scheme 3 Schematic diagram of photocatalytic degradation mechanism of MB by HEC/SiO_2/C_3N_4 under visible light irradiation.

band could not oxidize OH^- and H_2O to ·OH (Sheng et al., 2019). The reduction potential of the conduction band of g-C_3N_4 was more negative than that of $O_2/{}^{\cdot}O_2^-$ [$E^{\theta}(O_2/{}^{\cdot}O_2^-)$ = -0.33 eV], so the photogenerated electrons could reduce O_2 to ${}^{\cdot}O_2^-$. ${}^{\cdot}O_2^-$ presented strong oxidation capacity which oxidized and degraded the adsorbed dyes. It could be concluded that benefitting from the excellent adsorption capacity and good photocatalytic activity, the dyes could be removed efficiently by the porous HEC/SiO_2/C_3N_4 solid foam. The photocatalytic degradation mechanism of MB by HEC/SiO_2/C_3N_4 under visible light was shown in Scheme 3.

4. Conclusion

In the present study, novel hierarchical HEC/SiO_2/C_3N_4 solid foam was successfully fabricated with gas bubbles template and freeze-drying method for adsorption and photocatalytic degradation of organic dye in wastewater. Compared with the HEC/SiO_2/C_3N_4-50 foam without gas foaming, the HEC/SiO_2/C_3N_4-80 with air bubbles template showed higher porosity, larger specific surface area, higher pore volume, which were beneficial for the synergistic effect of adsorption capacity and photocatalytic activity. Compared with the powder g-C_3N_4, the obtained solid foams can be more easily separated from the wastewater. In summary, the designed hierarchical HEC/SiO_2/C_3N_4 solid foams will have broad application potential in treatment of organic dyes in wastewater.

Declaration of Competing Interest

The authors declare that they have no known competing financial interests or personal relationships that could have appeared to influence the work reported in this paper.

Acknowledgement

This work was supported by the Natural Science Foundation of Shandong Province (No. ZR2021QB178 and ZR2021QB197).

Appendix A. Supplementary material

Supplementary data to this article can be found online at https://doi.org/10.1016/j.arabjc.2022.104105.

References

Andrieux, S., Quell, A., Stubenrauch, C., et al, 2018. Liquid foam templating – a route to tailor-made polymer foams. Adv. Colloid Interface Sci. 256, 276–290. https://doi.org/10.1016/j.cis.2018.03.010.

Azizian, S., 2004. Kinetic models of sorption: a theoretical analysis. J. Colloid Interface Sci. 276, 47–52. https://doi.org/10.1016/j.jcis.2004.03.048.

Bagley, R.H.T., Jones, S.T., 2021. Deoxyribonucleic acid polymer nanoparticle hydrogels. Chem. Commun. 57, 12111–12114. https://doi.org/10.1039/d1cc05668a.

Bai, J., Zhou, A., Huang, Z., et al, 2015. Ultra-light and elastic graphene foams with a hierarchical structure and a high oil absorption capacity. J. Mater. Chem. A 3, 22687–22694. https://doi.org/10.1039/c5ta06204g.

Bao, L., Zhu, S., Chen, Y., et al, 2022. Anionic defects engineering of Co_3O_4 catalyst for toluene oxidation. Fuel 314,. https://doi.org/10.1016/j.fuel.2021.122774 122774.

Barbetta, A., Barigelli, E., Dentini, M., 2009. Porous alginate hydrogels: synthetic methods for tailoring the porous texture. Biomacromolecules 10, 2328–2337. https://doi.org/10.1021/bm900517q.

Chatterjee, S., Lee, D.S., Lee, M.W., et al, 2009. Enhanced adsorption of Congo red from aqueous solutions by chitosan hydrogel beads impregnated with cetyl trimethyl ammonium bromide. Bioresour Technol. 100, 2803–2809. https://doi.org/10.1016/j.biortech.2008.12.035.

Chaudhary, J., Thakur, S., Mamba, G., et al, 2021. Hydrogel of gelatin in the presence of graphite for the adsorption of dye: Towards the concept for water purification. J. Environ. Chem. Eng. 9,. https://doi.org/10.1016/j.jece.2020.104762 104762.

Dai, H., Huang, Y., Zhang, H., et al, 2020. Direct fabrication of hierarchically processed pineapple peel hydrogels for efficient Congo red adsorption. Carbohydr. Polym. 230,. https://doi.org/10.1016/j.carbpol.2019.115599 115599.

Das, S., Chakraborty, P., Ghosh, R., et al, 2017. Folic acid-polyaniline hybrid hydrogel for adsorption/reduction of chromium(VI) and selective adsorption of anionic dye from water. ACS Sustain. Chem. Eng. 5, 9325–9337. https://doi.org/10.1021/acssuschemeng.7b02342.

Eskhan, A., Banat, F., Selvaraj, M., et al, 2018. Enhanced removal of methyl violet 6B cationic dye from aqueous solutions using calcium alginate hydrogel grafted with poly (styrene-co-maleic anhydride). Polym. Bull. 76, 175–203. https://doi.org/10.1007/s00289-018-2378-y.

Gong, T., Hou, Y., Yang, X., et al, 2019. Gelation of hydroxyethyl cellulose aqueous solution induced by addition of colloidal silica nanoparticles. Int. J. Biol. Macromol. 134, 547–556. https://doi.org/10.1016/j.ijbiomac.2019.05.069.

Hao, Q., Chen, T., Wang, R., et al, 2018. A separation-free polyacrylamide/bentonite/graphitic carbon nitride hydrogel with excellent performance in water treatment. J. Clean. Prod. 197, 1222–1230. https://doi.org/10.1016/j.jclepro.2018.06.289.

Ho, Y., Porter, J., McKay, G., 2002. Equilibrium isotherm studies for the sorption of divalent metal ions onto peat: copper, nickel and lead single component systems. Water Air Soil Pollut. 141, 1–33. https://doi.org/10.1023/A:1021304828010.

Hou, C., Ma, K., Jiao, T., et al, 2016. Preparation and dye removal capacities of porous silver nanoparticle-containing composite hydrogels via poly (acrylic acid) and silver ions. RSC Adv. 6, 110799–110807. https://doi.org/10.1039/C6RA23371F.

Huang, Y., Yang, J., Chen, L., et al, 2018. Chitin nanofibrils to stabilize long-life pickering foams and their application for lightweight porous materials. ACS Sustain. Chem. Eng. 6, 10552–10561. https://doi.org/10.1021/acssuschemeng.8b01883.

Jiao, C., Li, T., Wang, J., et al, 2020. Efficient removal of dyes from aqueous solution by a porous sodium alginate/gelatin/graphene oxide triple-network composite aerogel. J. Polym. Environ. 28, 1492–1502. https://doi.org/10.1007/s10924-020-01702-1.

Jilal, I., El Barkany, S., Bahari, Z., et al, 2018. New quaternized cellulose based on hydroxyethyl cellulose (HEC) grafted EDTA: Synthesis, characterization and application for Pb (II) and Cu (II) removal. Carbohydr. Polym. 180, 156–167. https://doi.org/10.1016/j.carbpol.2017.10.012.

Jin, A., Liu, X., Li, M., et al, 2019. One-pot ionothermal synthesized carbon nitride heterojunction nanorods for simultaneous photocatalytic reduction and oxidation reactions: synergistic effect and mechanism insight. ACS Sustain. Chem. Eng. 7, 5122–5133. https://doi.org/10.1021/acssuschemeng.8b05969.

Kinniburgh, D.G., 1986. General purpose adsorption isotherms. Environ. Sci. Technol. 20, 895–904. https://doi.org/10.1021/es00151a008.

Lau, T.H.M., Wong, L.L.C., Lee, K.-Y., et al, 2014. Tailored for simplicity: creating high porosity, high performance bio-based macroporous polymers from foam templates. Green Chem. 16, 1931–1940. https://doi.org/10.1039/c3gc41807c.

Lesov, I., Tcholakova, S., Denkov, N., 2014. Factors controlling the formation and stability of foams used as precursors of porous materials. J. Colloid Interface Sci. 426, 9–21. https://doi.org/10.1016/j.jcis.2014.03.067.

Liu, R., Zhao, M., Zheng, X., et al, 2021. Reduced graphene oxide/TiO_2(B) immobilized on nylon membrane with enhanced photocatalytic performance. Sci. Total Environ. 799,. https://doi.org/10.1016/j.scitotenv.2021.149370 149370.

Liu, Y.-X., Zhong, H., Li, X.-R., et al, 2022. Fabrication of attapulgite-based dual responsive composite hydrogel and its efficient adsorption for methyl violet. Environ. Technol. 43, 1480–1492. https://doi.org/10.1080/09593330.2020.1838623.

Mandal, B., Ray, S.K., 2013. Synthesis of interpenetrating network hydrogel from poly (acrylic acid-co-hydroxyethyl methacrylate) and sodium alginate: Modeling and kinetics study for removal of synthetic dyes from water. Carbohydr. Polym. 98, 257–269. https://doi.org/10.1016/j.carbpol.2013.05.093.

Mokhtar, A., Abdelkrim, S., Djelad, A., et al, 2020. Adsorption behavior of cationic and anionic dyes on magadiite-chitosan composite beads. Carbohydr. Polym. 229,. https://doi.org/10.1016/j.carbpol.2019.115399 115399.

Mukerabigwi, J.F., Lei, S., Fan, L., et al, 2016. Eco-friendly nanohybrid superabsorbent composite from hydroxyethyl cellulose and diatomite. RSC Adv. 6, 31607–31618. https://doi.org/10.1039/c6ra01759b.

Nakhjiri, M.T., Marandi, G.B., Kurdtabar, M., 2018. Poly (AA-co-VPA) hydrogel cross-linked with N-maleyl chitosan as dye adsorbent: Isotherms, kinetics and thermodynamic investigation. Int. J. Biol. Macromol. 117, 152–166. https://doi.org/10.1016/j.ijbiomac.2018.05.140.

Nguyen, C.H., Juang, R.-S., 2019. Efficient removal of methylene blue dye by a hybrid adsorption–photocatalysis process using reduced graphene oxide/titanate nanotube composites for water reuse. J. Ind. Eng. Chem. 76, 296–309. https://doi.org/10.1016/j.jiec.2019.03.054.

Parlett, C.M.A., Wilson, K., Lee, A.F., 2013. Hierarchical porous materials: catalytic applications. Chem. Soc. Rev. 42, 3876–3893. https://doi.org/10.1039/c2cs35378d.

Qi, H., Ji, X., Shi, C., et al, 2019. Bio-templated 3D porous graphitic carbon nitride hybrid aerogel with enhanced charge carrier separation for efficient removal of hazardous organic pollutants. J Colloid Interface Sci. 556, 366–375. https://doi.org/10.1016/j.jcis.2019.08.072.

Qi, X., Li, Z., Shen, L., et al, 2019. Highly efficient dye decontamination via microbial salecan polysaccharide-based gels. Carbohydr. Polym. 219, 1–11. https://doi.org/10.1016/j.carbpol.2019.05.021.

Qian, D., Bai, L., Wang, Y.-S., et al, 2019. A bifunctional alginate-based composite hydrogel with synergistic pollutant adsorption and photocatalytic degradation performance. Ind. Eng. Chem. Res. 58, 13133–13144. https://doi.org/10.1021/acs.iecr.9b01709.

Ren, L., Xu, J., Zhang, Y., et al, 2019. Preparation and characterization of porous chitosan microspheres and adsorption performance for hexavalent chromium. Int. J. Biol. Macromol. 135, 898–906. https://doi.org/10.1016/j.ijbiomac.2019.06.007.

Rudzinski, W., Plazinski, W., 2006. Kinetics of solute adsorption at solid/solution interfaces: a theoretical development of the empirical pseudo-first and pseudo-second order kinetic rate equations, based on applying the statistical rate theory of interfacial transport. J. Phys. Chem. B 110, 16514–16525. https://doi.org/10.1021/jp061779n.

Sheng, Y., Wei, Z., Miao, H., et al, 2019. Enhanced organic pollutant photodegradation via adsorption/photocatalysis synergy using a 3D g-C_3N_4/TiO_2 free-separation photocatalyst. Chem. Eng. J. 370, 287–294. https://doi.org/10.1016/j.cej.2019.03.197.

Singha, N.R., Mahapatra, M., Karmakar, M., et al, 2017. Synthesis of guar gum-g-(acrylic acid-co-acrylamide-co-3-acrylamido propanoic acid) IPN via in situ attachment of acrylamido propanoic acid for analyzing superadsorption mechanism of Pb (II)/Cd (II)/Cu (II)/MB/MV. Polym. Chem. 8, 6750–6777. https://doi.org/10.1039/C7PY01564J.

Takeshita, J., Hasegawa, Y., Yanai, K., et al, 2017. Organic dye adsorption by amphiphilic tris-urea supramolecular hydrogel. Chem. - Asian J. 12, 2029–2032. https://doi.org/10.1002/asia.201700708.

Tan, H., Tu, S., Zhao, Y., et al, 2018. A simple and environment-friendly approach for synthesizing macroporous polymers from aqueous foams. J. Colloid Interface Sci. 509, 209–218. https://doi.org/10.1016/j.jcis.2017.09.018.

Tan, L., Yu, C., Wang, M., et al, 2019. Synergistic effect of adsorption and photocatalysis of 3D g-C_3N_4-agar hybrid aerogels. Appl. Surf. Sci. 467, 286–292. https://doi.org/10.1016/j.apsusc.2018.10.067.

Wang, H., Wu, Y., Feng, M., et al, 2018. Visible-light-driven removal of tetracycline antibiotics and reclamation of hydrogen energy from natural water matrices and wastewater by polymeric carbon nitride foam. Water Res. 144, 215–225. https://doi.org/10.1016/j.watres.2018.07.025.

Xu, J., Zhu, C., Song, S., et al, 2022. A nanocubicle-like 3D adsorbent fabricated by in situ growth of 2D heterostructures for removal of aromatic contaminants in water. J. Hazard. Mater. 423,. https://doi.org/10.1016/j.jhazmat.2021.127004 127004.

Yan, B., Chen, Z., Cai, L., et al, 2015. Fabrication of polyaniline hydrogel: synthesis, characterization and adsorption of methylene blue. Appl. Surf. Sci. 356, 39–47. https://doi.org/10.1016/j.apsusc.2015.08.024.

Yang, X.-Y., Chen, L.-H., Li, Y., et al, 2017. Hierarchically porous materials: synthesis strategies and structure design. Chem. Soc. Rev. 46, 481–558. https://doi.org/10.1039/c6cs00829a.

Yang, J., Li, Z., Zhu, H., 2017. Adsorption and photocatalytic degradation of sulfamethoxazole by a novel composite hydrogel with visible light irradiation. Appl. Catal. B 217, 603–614. https://doi.org/10.1016/j.apcatb.2017.06.029.

Yousefi, N., Wong, K.K.W., Hosseinidoust, Z., et al, 2018. Hierarchically porous, ultra-strong reduced graphene oxide-cellulose nanocrystal sponges for exceptional adsorption of water contaminants. Nanoscale 10, 7171–7184. https://doi.org/10.1039/c7nr09037d.

Zhang, Z., Tan, H., Zhao, Y., et al, 2019. Facile synthesis of macroporous zwitterionic hydrogels templated from graphene oxide-stabilized aqueous foams. J. Colloid Interface Sci. 553, 40–49. https://doi.org/10.1016/j.jcis.2019.06.022.

Zhang, X., Zhang, T., Wang, Z., et al, 2018. Ultralight, superelastic, and fatigue-resistant graphene aerogel templated by graphene oxide liquid crystal stabilized air bubbles. ACS Appl. Mater. Interfaces 11, 1303–1310. https://doi.org/10.1021/acsami.8b18606.

Zhao, H., Li, Y., 2020. Eco-friendly floatable foam hydrogel for the adsorption of heavy metal ions and use of the generated waste for the catalytic reduction of organic dyes. Soft Matter 16, 6914–6923. https://doi.org/10.1039/d0sm00756k.

Zhao, H., Qi, N., Li, Y., 2019. Interaction between polysaccharide monomer and SiO_2/Al_2O_3/$CaCO_3$ surfaces: a DFT theoretical study. Appl. Surf. Sci. 466, 607–614. https://doi.org/10.1016/j.apsusc.2018.10.085.

Zhou, L., Huang, J., He, B., et al, 2014. Peach gum for efficient removal of methylene blue and methyl violet dyes from aqueous solution. Carbohydr. Polym. 101, 574–581. https://doi.org/10.1016/j.carbpol.2013.09.093.

Zhu, C., Fang, Q., Liu, R., et al, 2022. Insights into the crucial role of electron and spin structures in heteroatom-doped covalent triazine frameworks for removing organic micropollutants. Environ. Sci. Technol. 56, 6699–6709. https://doi.org/10.1021/acs.est.2c01781.